Localized Collocation Meshless Method for Modeling Transdermal Pharmacokinetics in Multiphase Skin Structures

Presented by:

Eduardo Divo (ERAU-ME)

Collaborators:

Anthony Khoury (ERAU-ME), Vladimir Golubev (ERAU-AE), and Alain Kassab (UCF-MAE)

ERAU Math Department Colloquium

April 3, 2024

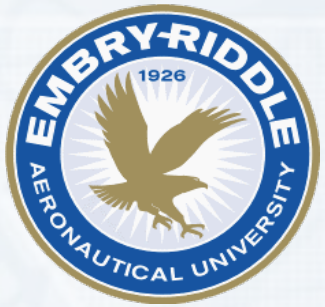

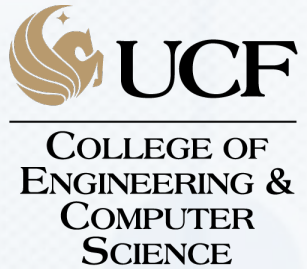

Introduction

- Human skin is a complex structure with different phenomena affecting the propagation of skin-injected substances, such as, partitioning, metabolic reactions, adsorption, and elimination.
- Additionally, the small physical dimensions and the large time scale of the problem incur further complexities in numerical modeling schemes
- Thus, it is believed that modeling of the transdermal drug delivery process can be improved by implementing meshless methods, which carry certain advantages in addressing these complications
- Here, the Localized Collocation Meshless Method is compared to published results from a commercial software package, SKIN-CAD® as well as experimental results

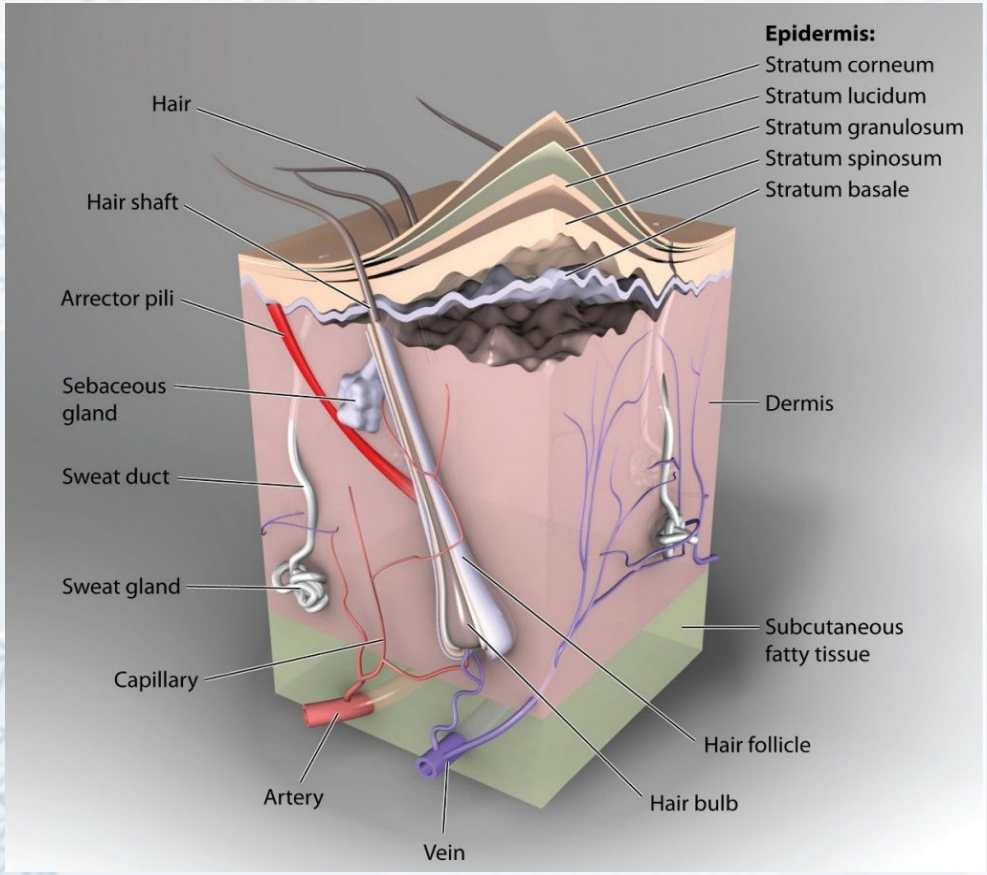

Figure 1: Skin structure [1]

Pharmacokinetic Modeling

- Following Al-Qallaf, et al, an extended version of Fick's second law governing the process of compound diffusion is employed in a multilayer, two-compartment model
  - Layers: Stratum Corneum, Viable Epidermis and Dermis
  - Compartments: Blood and tissue
- Considered method of compound delivery is direct needle injection into the dermis
  - Bypassing the stratum corneum allows us to model the diffusive and metabolic process in viable tissue and blood compartments only.
  - Improves numerical predictions that rely on various uncertain, empirically determined parameters affecting skin dynamic processes.

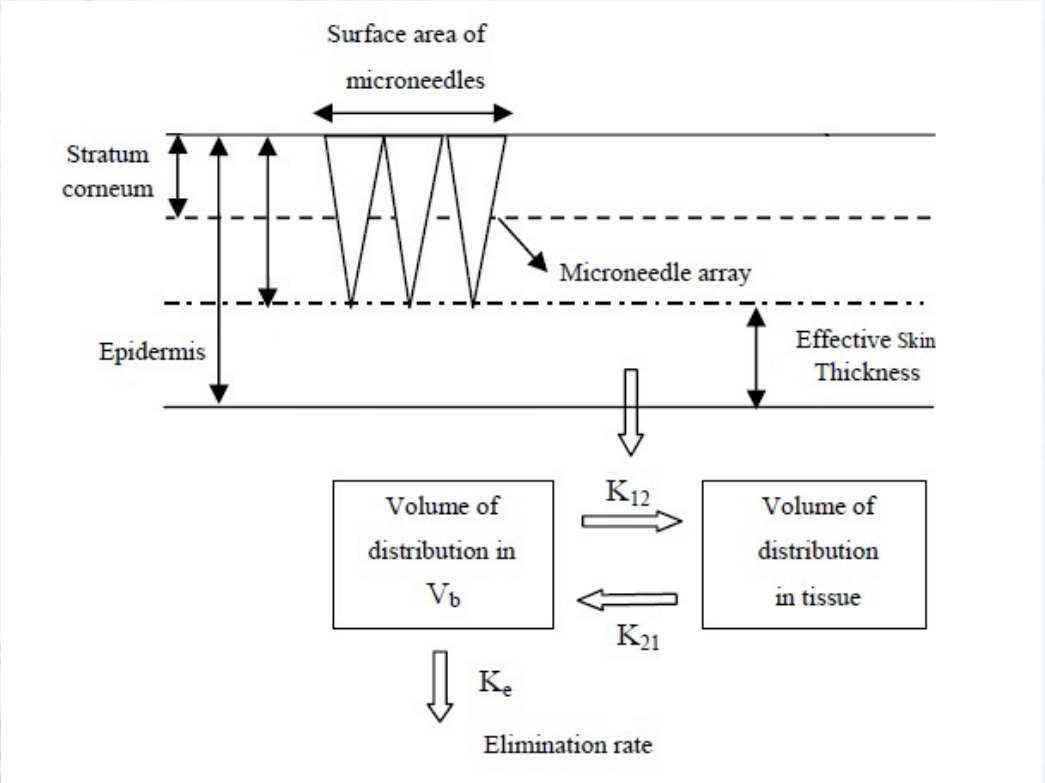

Figure 2: Transdermal Drug Delivery (TDD) Schematic

Mathematical Formulation for Skin Model

- In general, the one-dimensional flux per unit area, J, of substance transport by diffusion through a solvent follows Fick's First Law:

$$J = -D\frac{\partial c}{\partial x}$$

- Accounting for conservation of mass of the substance, we arrive at Fick's Second Law:

$$\frac{\partial c}{\partial t} = D\frac{\partial^2 c}{\partial x^2}, \text{ (in 1D)} \quad \text{and} \quad \frac{\partial c}{\partial t} = D\nabla^2 c, \text{ (in 2D+)}$$

- Considering first-order metabolic effects:

$$\frac{\partial c}{\partial t} = D\nabla^2 c - Kc$$

- Finally, assuming linear coupling between substance concentrations that are bound and unbound with blood:

$$\frac{\partial c}{\partial t} = D\nabla^2 c + \left(K_{12}c_b\frac{V_b}{V_t} - K_{21}c\right) - Kc$$

$$\frac{dc_b}{dt} = \left(K_{21}c\frac{V_t}{V_b} - K_{12}c_b\right) - K_e c_b$$

- Where:
  - c, c_b – drug concentration in tissue and blood compartments *(kg/m³)*
  - D – diffusion coefficient *(m²/s)*
  - K – metabolic reaction rate constant *(1/s)*
  - K_e – elimination rate constant *(1/s)*
  - V_t, V_b – volumes of tissue and blood *(m³)*
  - K_{12}, K_{21} – binding and unbinding rate constants *(1/s)*

A Brief Introduction on Meshless Methods

- The term “meshless” refers to a class of methods that do not require boundary and/or interior point discretization, polygonization, integration or point ordering structure (as in FDM)
- The RBF-based Localized Collocation Meshless Method, as extended from the Kansa Method uses a scattered, non-ordered point distribution throughout the domain and boundary to approximate differential operators in the governing equation

Radial-basis Function Interpolation

- For this purpose, assume some domain, Ω, with boundary Γ
- Assume a finite number of points, *NB*, used as ‘data centers’ on the boundary
- Assume a finite number of points, *NI*, used as ‘data centers’ inside the domain of interest
- Resulting in a total number of points: N = NB + NI

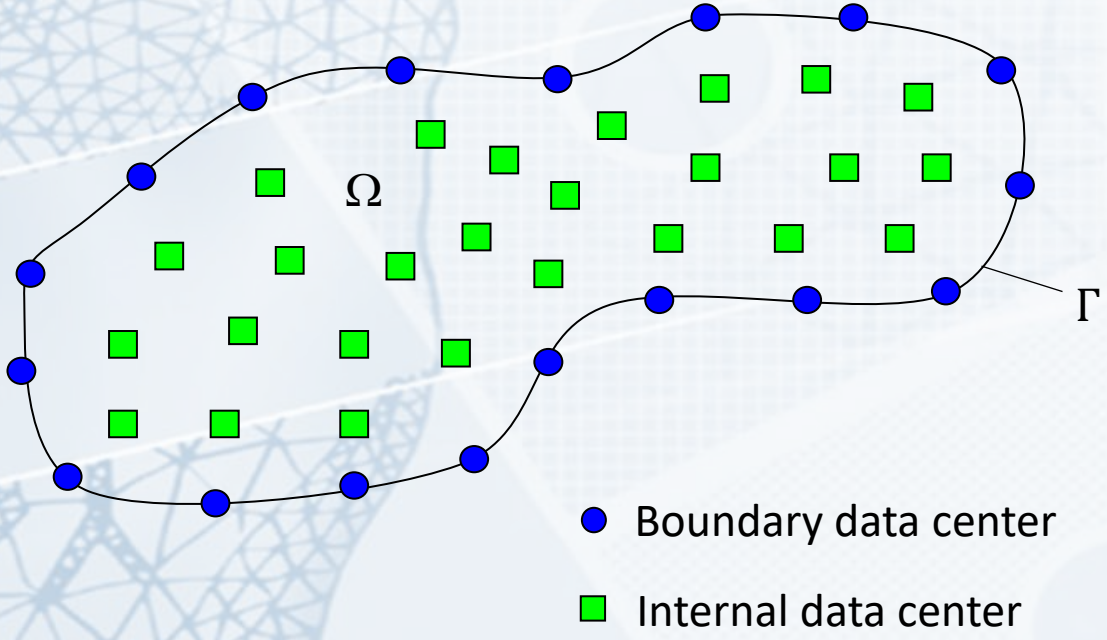

Figure 3: Domain and Boundary with Data Centers

Radial-basis Function Interpolation

- Assume a general field variable may be interpolated in terms of a finite number of expansion functions as:

$$c(x) = \sum_{j=1}^{N} \alpha_j \chi_j(x)$$

- Where:
  - x – generalized spatial coordinates, in 2D, (x,y)
  - c – field variable (here, drug concentration)
  - α – expansion coefficients
  - χ – arbitrary (prescribed) expansion functions

- This proposed expansion will later be introduced into the governing equations for the problem at hand

Radial-basis Function Interpolation

- The expansion functions may be defined to belong to the family of Radial-Basis functions (RBF)
- Such functions consist of algebraic expressions uniquely defined in terms of Euclidean distance from an ‘expansion point’ or ‘data center’ to some general field point
- Many examples, but implemented here are inverse multiquadric RBF

$$\chi_j(x) = \left[\left(\frac{r_j}{\sigma}\right)^2 + 1\right]^{-1/2}$$

- Where:
  - r_j – Euclidean distance from expansion point

$$r_j = \sqrt{(x - x_j)^2 + (y - y_j)^2} \text{ in 2D}$$

  - x_j, y_j – location of expansion point j
  - σ – shape parameter
    - Of paramount importance; affects the flatness of the basis function and is optimized for solution

Radial-basis Function Interpolation

- From the expansion, field derivatives can be approximated by simple derivation of the interpolation function, χ_j, i.e.,

$$\frac{\partial c}{\partial x} = \sum_{j=1}^{N} \alpha_j \frac{\partial \chi_j}{\partial x}$$

- Thus, the Laplacian is,

$$\nabla^2 c = \sum_{j=1}^{N} \alpha_j \nabla^2 \chi_j$$

- And normal derivatives are,

$$\frac{\partial c}{\partial n} = \sum_{j=1}^{N} \alpha_j \frac{\partial \chi_j}{\partial n}$$

Radial-basis Function Interpolation

- Recalling the expansion,

$$c(x) = \sum_{j=1}^{N} \alpha_j \chi_j(x)$$

- This can be introduced into the generalized boundary condition,

$$\gamma_1 \, c(x)\Big|_\Gamma + \gamma_2 \frac{\partial c}{\partial n}(x)\Big|_\Gamma = \gamma_3\Big|_\Gamma$$

- such that,

$$\gamma_1 \sum_{j=1}^{N} \alpha_j \chi_j(x)\Big|_\Gamma + \gamma_2 \sum_{j=1}^{N} \alpha_j \frac{\partial \chi_j}{\partial n}(x)\Big|_\Gamma = \gamma_3\Big|_\Gamma$$

- This can be reduced to:

$$\sum_{j=1}^{N} \alpha_j \psi_j(x)\Big|_\Gamma = \gamma_3\Big|_\Gamma$$

Radial-basis Function Interpolation

- From the generalized boundary condition,

$$\gamma_1 \, c(x)\Big|_{\Gamma} + \gamma_2 \frac{\partial c}{\partial n}(x)\Big|_{\Gamma} = \gamma_3$$

  - 1st kind boundary conditions:

$$c\Big|_{\Gamma_1} = \sum_{j=1}^{N} \alpha_j \chi_j = \hat{c} \qquad \therefore \gamma_1 = 1, \gamma_2 = 0, \gamma_3 = \hat{c}$$

  - 2nd kind boundary conditions:

$$\frac{\partial c}{\partial n}\Big|_{\Gamma_2} = \sum_{j=1}^{N} \alpha_j \frac{\partial \chi_j}{\partial n} = \frac{-1}{D}\hat{J} \qquad \therefore \gamma_1 = 0, \gamma_2 = -D, \gamma_3 = \hat{J}$$

Radial-basis Function Interpolation

- Recalling the expansion,

$$c(x) = \sum_{j=1}^{N} \alpha_j \chi_j(x)$$

- Using the steady-state, uncoupled problem to demonstrate, this can also be introduced into governing equations such that,

$$D\nabla^2 c - Kc = 0$$

$$D\sum_{j=1}^{N} \alpha_j \nabla^2 \chi_j(x) - K\sum_{j=1}^{N} \alpha_j \chi_j(x) = 0$$

$$\sum_{j=1}^{N} \alpha_j \left[D\nabla^2 \chi_j(x) - K\chi_j(x) \right] = 0$$

- This can be reduced to:

$$\sum_{j=1}^{N} \alpha_j \phi_j(x) = 0$$

Radial-basis Function Interpolation

- Collocating the expanded boundary condition equation at the *NB* boundary data centers and the expanded governing equation at the *NI* internal data centers leads to square linear algebraic set for the expansion coefficients as:

$$\underline{\underline{A}}\,\underline{\alpha} = \underline{b}$$

- Where,

$$\underline{\underline{A}} = \begin{bmatrix} \psi_j(x_i) \\ \phi_j(x_i) \end{bmatrix}_{NB+NI}$$

$$\underline{b} = \begin{Bmatrix} \gamma_3 \\ 0 \end{Bmatrix}_{NB+NI}$$

- Leading to a solution for the expansion coefficients, $\underline{\alpha}$ by,

$$\underline{\alpha} = \underline{\underline{A}}^{-1}\underline{b}$$

Localized Collocation

- Despite the apparent accuracy and robustness of the Global RBF Meshless approach the issues of ill-conditioning and high memory and CPU power demands become notorious as the size of the problem increases particularly when dealing with 3D large-scale problems
- It becomes imperative to mitigate these issues, and is possible through localized expansion
- Rather than interpolating globally, the RBF interpolation is performed over local topologies of influence points with a handful of advantages
  - Optimization of each local interpolation (shape parameter, σ)
  - Reduces CPU and memory demands
  - Can be implemented without user intervention, automating the process

Localized Collocation

- Localized RBF interpolation is based on the selection of localized topologies of influence points as follows:
- The localized topology of NF influence points is automatically generated around each data center x_c
- The RBF interpolation of a function $\phi(x)$ is performed over NF influence points in the topology of a data center x_c. In addition, a series of NP polynomials $P_j(x)$ may be added to the expansion to ensure exact interpolation of constant and linear fields

$$\phi(\boldsymbol{x}) = \sum_{j=1}^{NF} \alpha_j \chi_j(\boldsymbol{x}) + \sum_{j=1}^{NP} \alpha_{j+NF} P_j(\boldsymbol{x}) \qquad \text{Where, } \{\phi\} = \begin{pmatrix} \phi(\boldsymbol{x}_1) \\ \vdots \\ \phi(\boldsymbol{x}_{NF}) \\ 0 \\ \vdots \\ 0 \end{pmatrix}$$

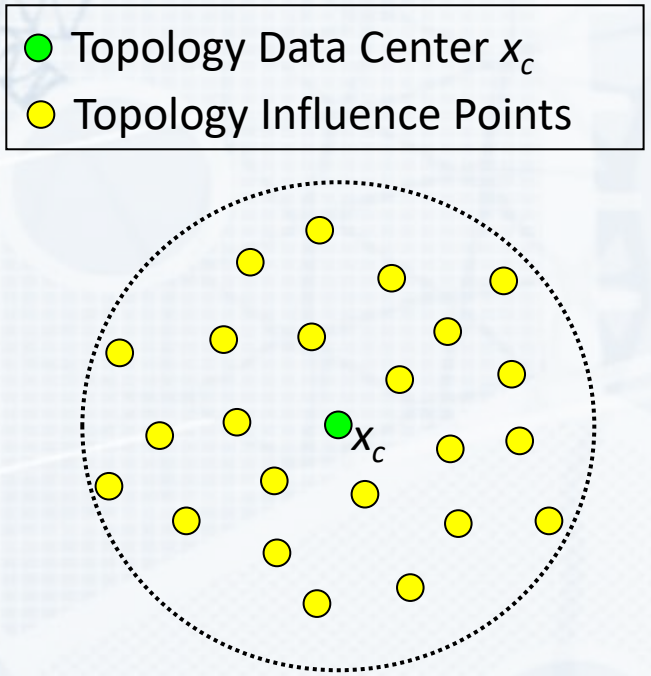

Figure 4: Localized Influence Topology

Localized Collocation

- Following a similar process as before, the expansion coefficients, α, may be determined as:

$$\{\phi\} = [C]\{\alpha\} \rightarrow \{\alpha\} = [C]^{-1}\{\phi\}$$

$$\text{Where, } [C] = \begin{bmatrix} \chi_1(\boldsymbol{x}_1) & \cdots & \chi_{NF}(\boldsymbol{x}_1) & P_1(\boldsymbol{x}_1) & \cdots & P_{NP}(\boldsymbol{x}_1) \\ \vdots & \ddots & \vdots & \vdots & \ddots & \vdots \\ \chi_1(\boldsymbol{x}_{NF}) & \cdots & \chi_j(\boldsymbol{x}_{NF}) & P_1(\boldsymbol{x}_{NF}) & \cdots & P_{NP}(\boldsymbol{x}_{NF}) \\ P_1(\boldsymbol{x}_1) & \cdots & P_1(\boldsymbol{x}_1) & 0 & \cdots & 0 \\ \vdots & \ddots & \vdots & \vdots & \ddots & \vdots \\ P_{NP}(\boldsymbol{x}_{NF}) & \cdots & P_{NP}(\boldsymbol{x}_{NF}) & 0 & \cdots & 0 \end{bmatrix} \; and \; \{\phi\} = \begin{pmatrix} \phi(\boldsymbol{x}_1) \\ \vdots \\ \phi(\boldsymbol{x}_{NF}) \\ 0 \\ \vdots \\ 0 \end{pmatrix}$$

Localized Collocation

- And test function derivatives at the data center, x_c, can be found in a similar manner to those derivatives found for globally interpolated RBF, where the linear derivative operator, $\mathcal{L}$, is applied to the expansion as follows:

$$\mathcal{L}\phi(\boldsymbol{x}_c) = \sum_{j=1}^{NF} \alpha_j \mathcal{L}\chi_j(\boldsymbol{x}_c) + \sum_{j=1}^{NP} \alpha_{j+NF} \mathcal{L}P_j(\boldsymbol{x}_c)$$

- And thus, in matrix form,

$$\mathcal{L}\phi_c = \{\mathcal{L}_c\}^T\{\alpha\} \rightarrow \mathcal{L}\phi_c = \{\mathcal{L}_c\}^T[C]^{-1}\{\phi\} \qquad \text{Where, } \{\mathcal{L}_c\} = \begin{pmatrix} \mathcal{L}\chi_1(\boldsymbol{x}_c) \\ \vdots \\ \mathcal{L}\chi_{NF}(\boldsymbol{x}_c) \\ \mathcal{L}P_1(\boldsymbol{x}_c) \\ \vdots \\ \mathcal{L}P_{NP}(\boldsymbol{x}_c) \end{pmatrix}$$

Transient Solution

- The formulation of the Localized Collocation Meshless Method (LCMM) for transient problems follows a first-order forward differencing approximation of the time derivative to formulate an explicit (Euler) integration scheme as:

$$c^{(k+1)} = c^{(k)} + \Delta t \left[D\nabla^2 c^{(k)} + \left(K_{12} c_b^{(k)} \frac{V_b}{V_t} - K_{21} c^{(k)} \right) - K c^{(k)} \right]$$

- Where the RBF interpolation of the field variable at the current time step (k) can be implemented to approximate the right-hand side of the discretized equation:

$$c^{(k+1)} = c^{(k)} + \Delta t \left[D \sum_{j=1}^{N} \alpha_j^{(k)} \nabla^2 \chi_j(x) + \left(K_{12} c_b^{(k)} \frac{V_b}{V_t} - K_{21} \sum_{j=1}^{N} \alpha_j^{(k)} \chi_j(x) \right) - K \sum_{j=1}^{N} \alpha_j^{(k)} \chi_j(x) \right]$$

- Notice that as the field evolves in time, only the expansion coefficients need to be updated at each time step (the RBF interpolation remains unchanged)

Transient Solution

- As the field solution is based on a set of two, linearly coupled equations, they must be simultaneously solved for to advance in time, where,

$$c^{(k+1)} = c^{(k)} + \Delta t \left[D\nabla^2 c^{(k)} + \left(K_{12} c_b^{(k)} \frac{V_b}{V_t} - K_{21} c^{(k)} \right) - K c^{(k)} \right]$$

$$c_b^{(k+1)} = c_b^{(k)} + \Delta t \left[\left(K_{21} c^{(k)} \frac{V_t}{V_b} - K_{12} c_b^{(k)} \right) - K_e c_b^{(k)} \right]$$

- Again, implementing the RBF interpolation of the field variable to approximate the RHS of the discretized equations
  - Note, that the drug concentration in the blood compartment, c_b, is effectively a 1st order time-varying ODE, but inherits spatial dimensionality by its dependence on the concentration in the tissue compartment

Pharmacokinetic Parameters

- LCMM is used to model diffusion of **Verapamil** (a calcium channel blocker used for treatment of HBP, angina, tachycardia, migraines, and other afflictions) given the extent of experimental work on identifying pharmacokinetic parameters, as well as traditional numerical models of Verapamil in the literature
- Recall Verapamil is delivered by microneedle array, and so pharmacokinetic parameters are required for Verapamil in the **viable epidermis** only
- The pharmacokinetic parameters required are:
  - D – diffusion coefficient *(m^2/s)*
  - K – metabolic reaction rate constant *(1/s)*
  - K_e – elimination rate constant *(1/s)*
  - V_t, V_b – volumes of tissue and blood *(m^3)*
  - K_{12}, K_{21} – binding and unbinding rate constants *(1/s)*

Pharmacokinetic Parameters

- Verapamil:
  - Diffusion coefficient, $D = 7.8 \cdot 10^{-8}\ [cm^2/s]$
  - Metabolic reaction rate constant, $K = 5.61 \cdot 10^{-4}\ [1/s]$
- Three experiments by Anderson et al., Eichelbaum et al. and Koike et al. give values for:
  - the elimination rate constant (K_e)
  - binding and unbinding rate constants (K_{12}, K_{21})
  - and the volume distribution of tissue and blood (V_t, V_b)

Pharmacokinetic Parameters

	K_e [1/s] ($\times 10^{-4}$)	K_{12} [1/s] ($\times 10^{-4}$)	K_{21} [1/s] ($\times 10^{-4}$)	V_t [mL] ($\times 10^{4}$)	V_b [mL] ($\times 10^{4}$)
Anderson, et al	1.58	2.19	1.11	5.18	2.63
Eichelbaum, et al	0.79	2.12	2.78	13.14	27.39
Koike, et al	1.5	6.22	3.94	8.34	6.47

Pharmacokinetic Parameters

- In Al Qallaf et al, six different cases were modeled; two for each of the three experimentally derived sets of pharmacokinetic parameters
  - One case with metabolic effects, $K = 5.61 \cdot 10^{-4}\ [1/s]$
  - One case without metabolic effects, $K = 0.0\ [1/s]$

Test Cases

Case	K [1/s] ($x10^{-4}$)	K_e [1/s] ($x10^{-4}$)	K_{12} [1/s] ($x10^{-4}$)	K_{21} [1/s] ($x10^{-4}$)	V_t [mL] ($x10^{4}$)	V_b [mL] ($x10^{4}$)
1	0	1.58	2.19	1.11	5.18	2.63
2	5.61	1.58	2.19	1.11	5.18	2.63
3	0	0.79	2.12	2.78	13.14	27.39
4	5.61	0.79	2.12	2.78	13.14	27.39
5	0	1.5	6.22	3.94	8.34	6.47
6	5.61	1.5	6.22	3.94	8.34	6.47

Computational Domain

- The 2D computational domain models the planar region surrounding a single microneedle within the microneedle array
- To reiterate, as the Verapamil is delivered via microneedle injection, diffusion through the stratum corneum can be neglected
- Additionally, the assumption is made that there is no back-propagation of Verapamil into the stratum corneum, given it's low permeability

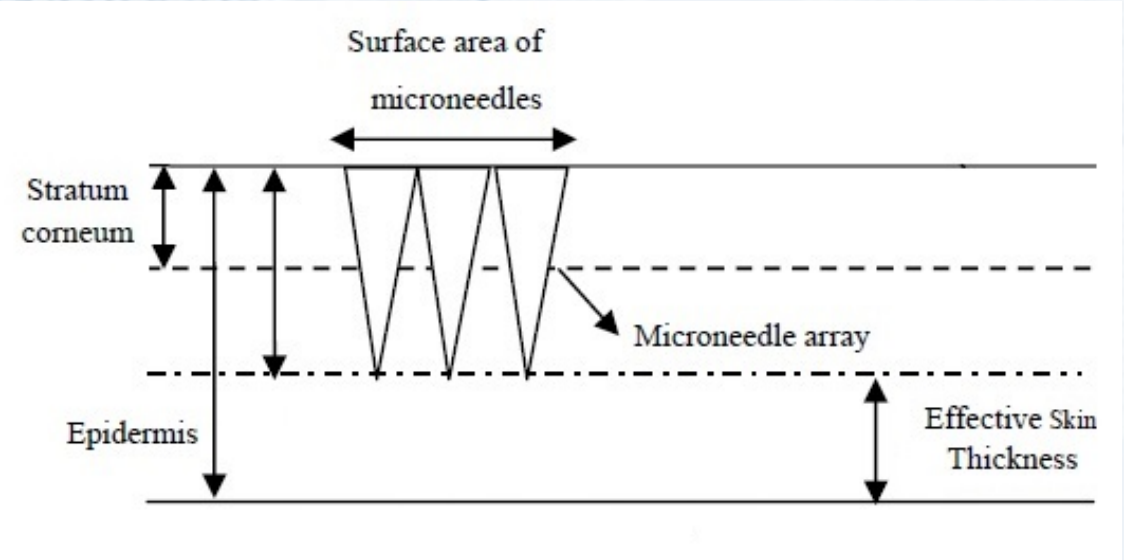

Figure 5: Microneedle Configuration in Model Schematic

Computational Domain

- Thus, the 2D computational domain is given with the following dimensions, boundary conditions and boundary condition values.

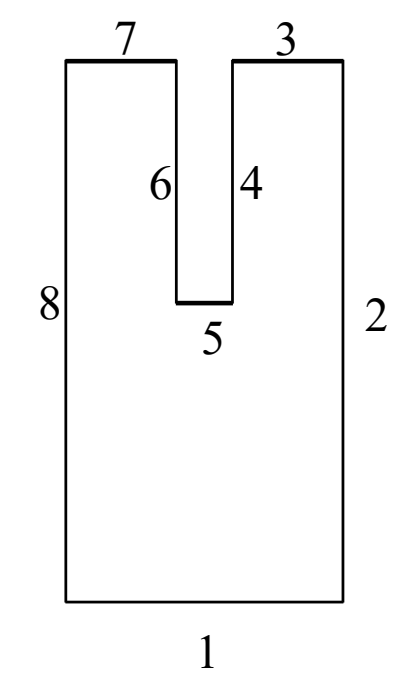

Index	Length [cm]	Boundary Condition	Boundary Value
1	0.025	1st Kind	0 $mg \cdot mL^{-1}$
2	0.036	Symmetry, 2nd Kind	0 $mg \cdot mL^{-1} \cdot cm^{-1}$
3	0.01	2nd Kind	0 $mg \cdot mL^{-1} \cdot cm^{-1}$
4	0.016	1st Kind	0 $mg \cdot mL^{-1}$
5	0.005	1st Kind	c_{needle}
6	0.016	1st Kind	0 $mg \cdot mL^{-1}$
7	0.01	2nd Kind	0 $mg \cdot mL^{-1} \cdot cm^{-1}$
8	0.036	Symmetry, 2nd Kind	0 $mg \cdot mL^{-1} \cdot cm^{-1}$

Figure 6: Simplified 2D Computation Domain

Computational Domain

- The data centers are distributed with an average spacing of:

$$\Delta x = \Delta y = 0.001\ cm$$

- Considering Fourier stability limits, the time step was:

$$\Delta t = 0.01\ seconds$$
$$t \in [0:8]\ hours$$

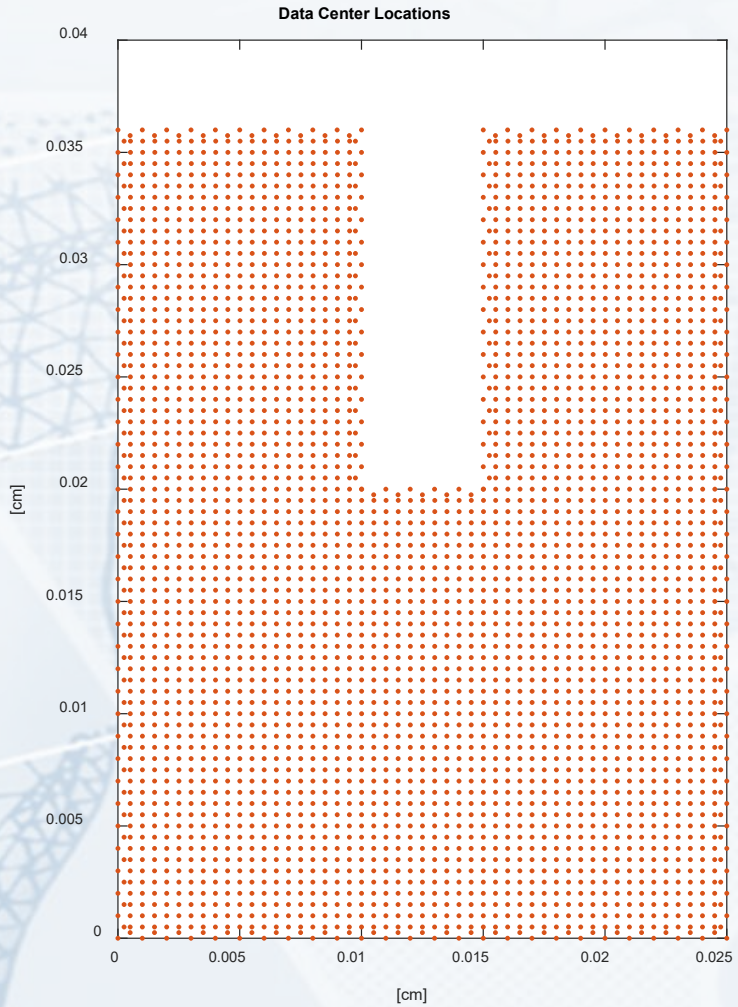

Figure 7: 2D Domain with Data Centers

Computational Domain

- Where the boundary condition at the microneedle tip is meant to match the prescribed substance input concentration time history such that:

$$c_{needle} = \begin{cases} 43\frac{mg}{mL} & if\ 0 < t \leq 4\ hours \\ 0\frac{mg}{mL} & if\ t > 4\ hours \end{cases}$$

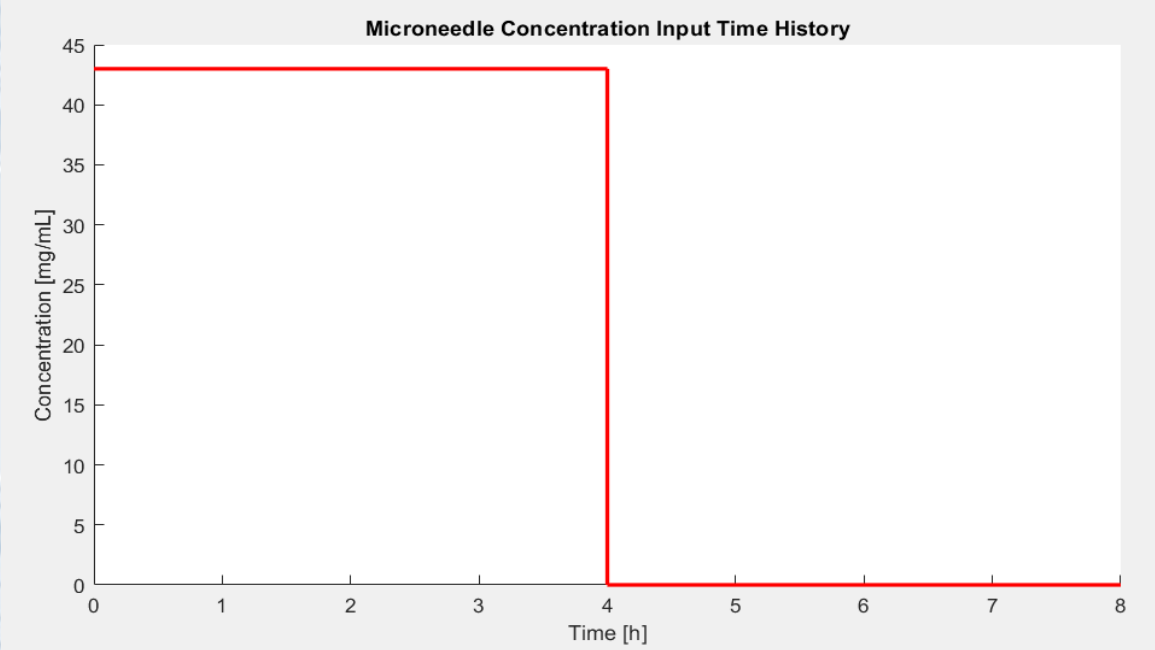

Figure 8: Microneedle Concentration Boundary Input

Numerical Results

- The time-accurate field solution for case 6 is given below

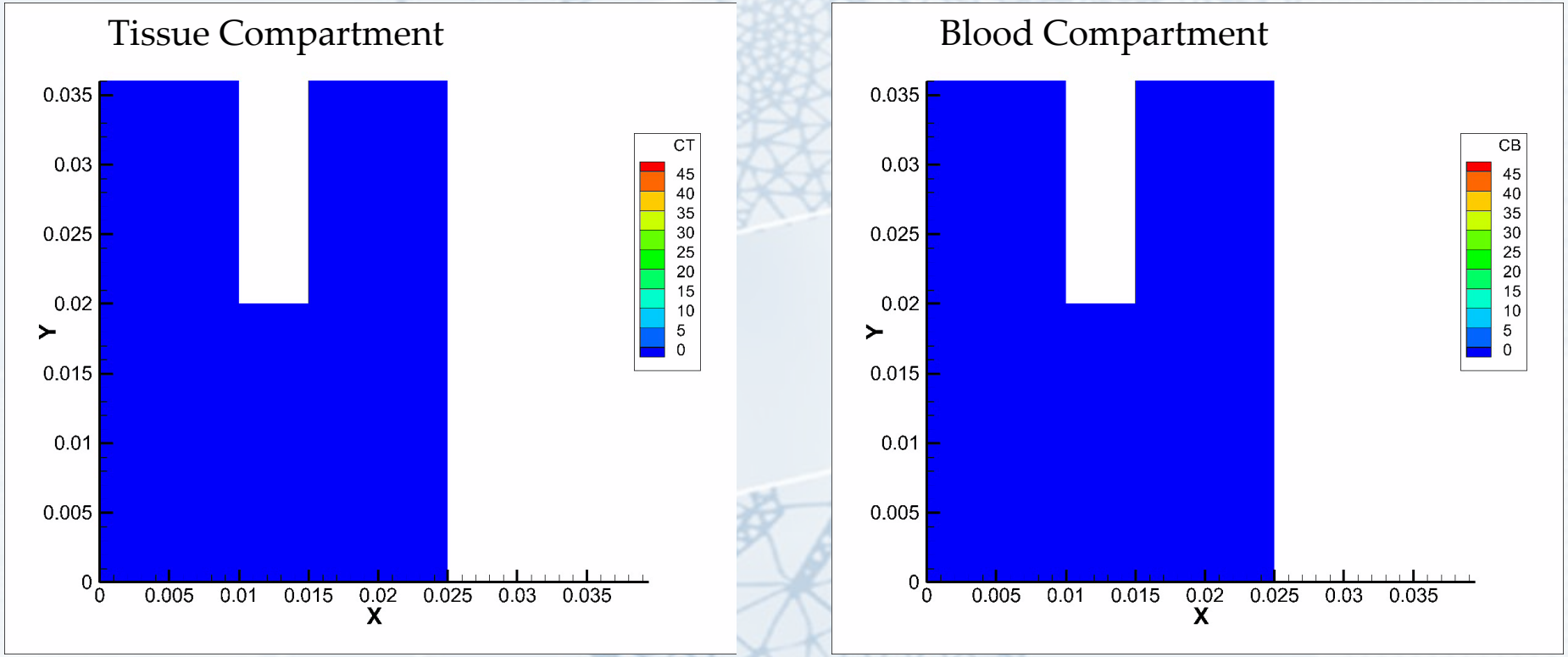

Figure 9: Field Solution for Verapamil Concentration in the Blood and Tissue Compartments

Numerical Results

- Previous numerical models were 1D field solutions, and experimental results are effectively 0D in space, only measuring blood concentrations over time
- Thus, to gauge the accuracy of results, we observe over the 8-hour time history:
  - Verapamil concentration in blood
  - Cumulative permeated Verapamil from the microneedle

Numerical Results:

Verapamil Concentration in Blood

- Volume averaged concentration of Verapamil in the blood compartment
- The time-history trend appears accurate, while also matching maximum values for all cases compared to 1D numerical results from Al Qallaf

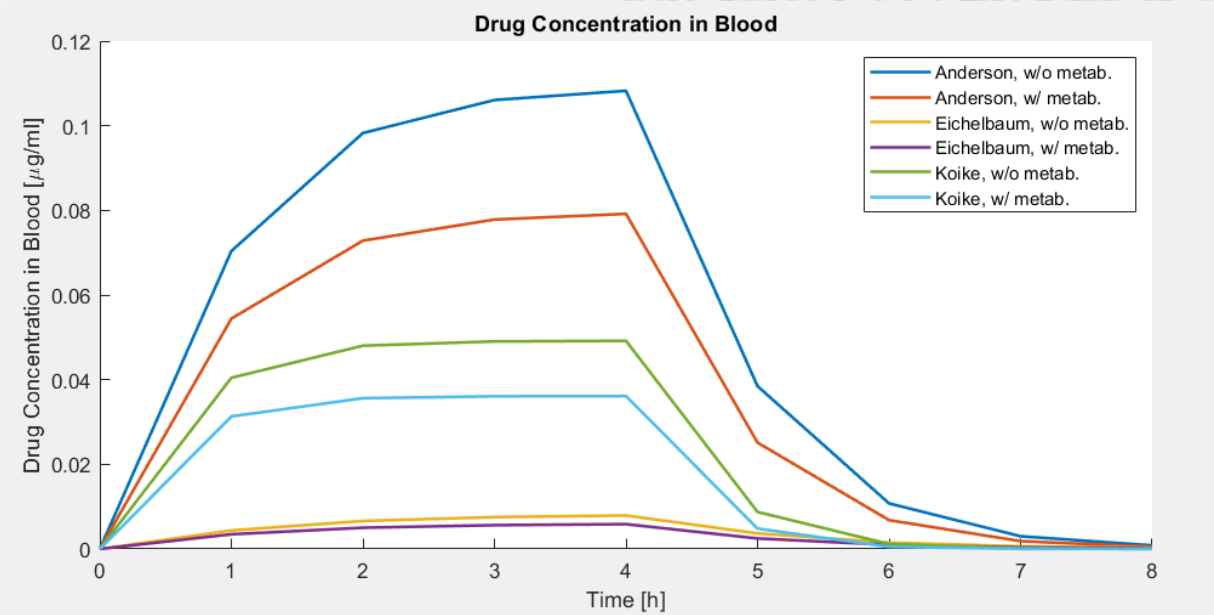

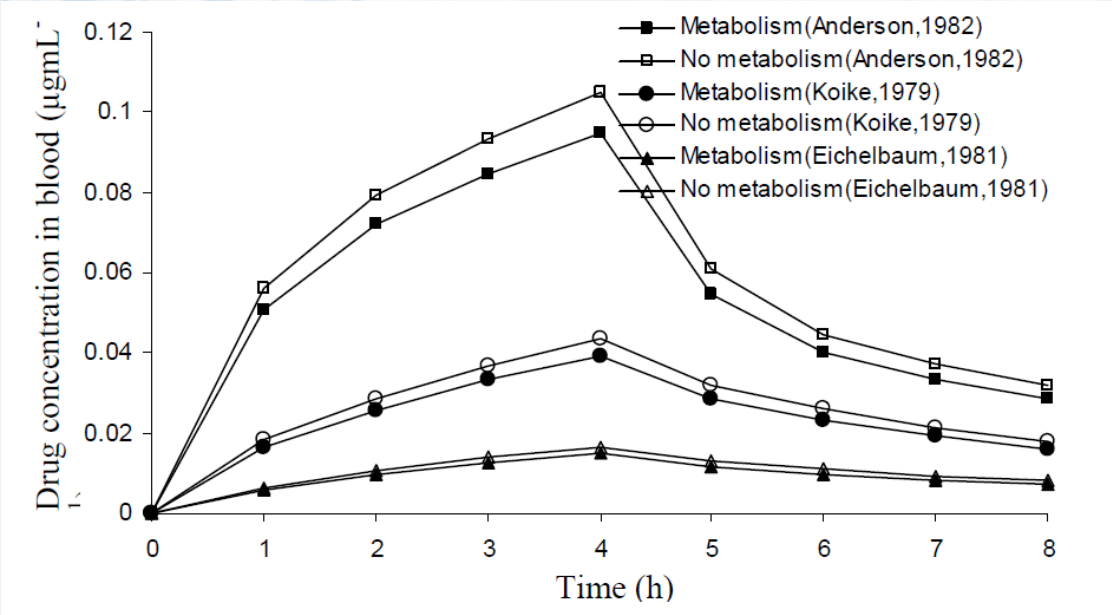

Figure 10: Verapamil Concentration in Blood from (a) 2D LCMM Model and (b) 1D SKIN-CAD® Model

Numerical Results:

Cumulative Permeated Verapamil

- Integrated flux at the tip of the microneedle; accumulated Verapamil concentration entering the tissue compartment
- Likewise, the time-history trend appears similar to the 1D numerical results from Al Qallaf however there are some discrepancies; (1) maximum value and (2) trend after 4 hours

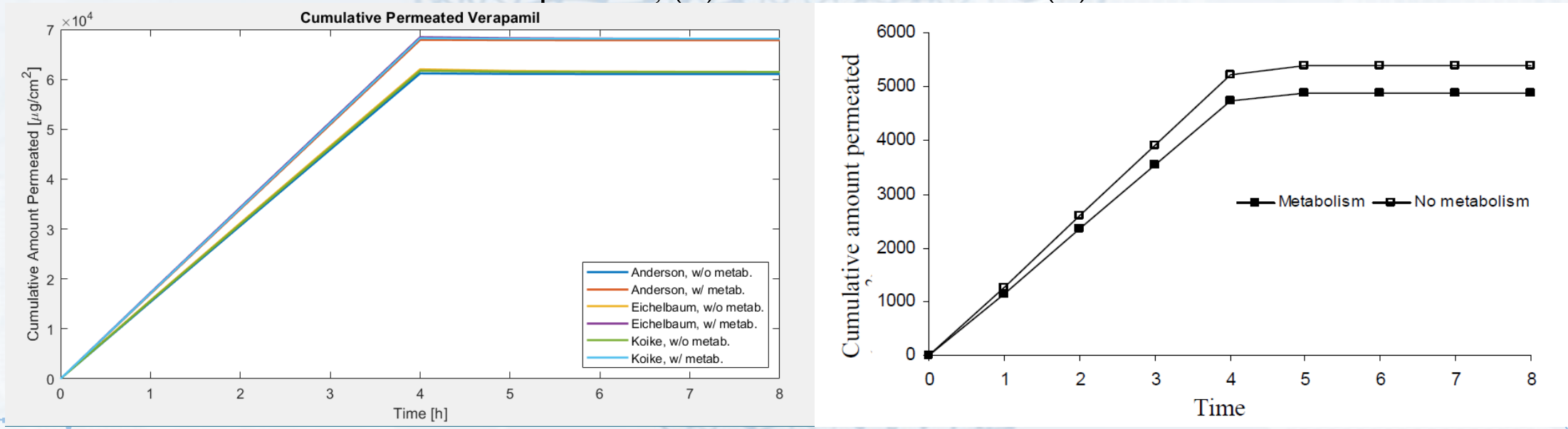

Figure 11: Cumulative Permeated Verapamil from (a) 2D LCMM Model and (b) 1D SKIN-CAD® Model

Numerical Results:

Cumulative Permeated Verapamil

- Increasing vs. decreasing values after 4 hours
  - At 4 hours, the microneedle concentration, c_{needle}, falls to 0 mg/mL
  - Thus, Verapamil can no longer enter the control volume, and flux at the surface must invert
  - This indicates that the LCMM model is capable of capturing behavior not observed in the 1D model
- Maximum values discrepancies may be a consequence of:
  - Average spacing: affects numerical derivative approximation

    and
  - 1D vs. 2D boundary conditions: affects accumulation of Verapamil in volume and the resulting gradient

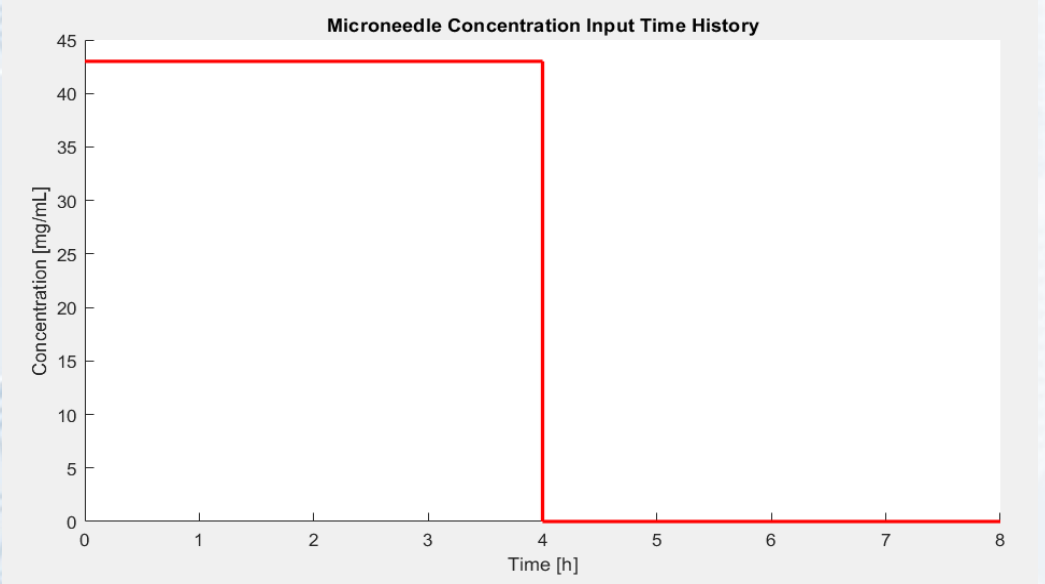

Figure 12: Microneedle Concentration Boundary Input

Acknowledgments

Vladimir Golubev and the group would like to acknowledge support from the ABG Lab for help in completing this work

References

- Pepper, D., Kassab, A., and Divo, E., An Introduction to Finite Element, Boundary Element, and Meshless Methods: with Applications to Heat Transfer and Fluid Flow. ASME Press, 2014.

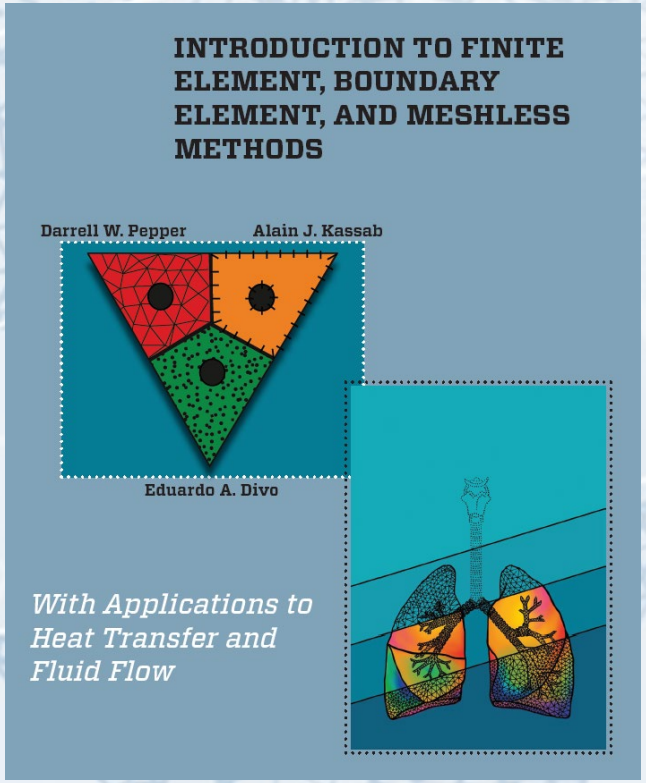

References

- Khoury, A., Golubev, V., Kassab, A., and, Divo, E. “Pharmacokinetic Parameter Identification using a Meshless Method Approach for Transdermal Drug Delivery,” Engineering Analysis with Boundary Elements, 150, 94-102, (2023).
- Khoury, A., Divo, E., Golubev, V., and Kassab, A. “Meshless modeling of coupled transdermal pharmacokinetics with analytical validation,” Engineering Analysis with Boundary Elements, 122 (2021) 62–74.
- Das, A., Khoury, A., Divo, E., Huayamave, V., Ceballos, A., Eaglin, R., Kassab, A., Payne, A., Yelandur, V., and Seigneur, H., “Real-Time Thermomechanical Modeling of PV Cell Fabrication via a POD-Trained RBF Interpolation Network,” CMES-Computer Modeling in Engineering & Sciences Volume 122, Number 3, pp 757-777, 2020.
- Khoury, A.; Divo, E.; Kassab, A.; Kakuturu, S.; Reddi, L. Meshless Modeling of Flow Dispersion and Progressive Piping in Poroelastic Levees. Fluids 2019, 4(3), 120
- De Montea, F., et al. Chapter 10: Transdermal Drug Delivery and Percutaneous Absorption. In: Heat Transfer and Fluid Flow in Biological Processes, 273-304, 2015.
- Millington P. F., Wilkinson R. Skin. Cambridge University Press, 2009.
- Roberts M. S., et al. Skin transport. In: Dermatological and transdermal formulations. Boca Raton: CRC Press, 2002.
- Streng W. H. Partition coefficient. In: Characterization of compounds in solution (Theory and Practise). USA: Springer, 47-60, 2001.

References

- Anissimov, Y. G., Roberts, M. S. Diffusion modelling of percutaneous absorption kinetics: 4. Effects of a slow equilibration process within stratum corneum on absorption and desorption kinetics. J Pharm Sci, 98:772-81, 2009.
- Roberts M. S., et al. Basic mathematical principles in skin permeation. In: Dermatological and transdermal formulations. CRC Press, 2002.
- Anissimov, Y. G., Roberts, M. S. Diffusion modeling of percutaneous absorption kinetics: 3. Variable diffusion and partition coefficients, consequences for stratum corneum depth profiles and desorption kinetics. J Pharm Sci, 93:470-87, 2004.
- Anissimov, Y. G., et al. Mathematical and pharmacokinetic modelling of epidermal and dermal transport processes. Adv Drug Deliv Rev, 65:169-90, 2013.
- Naegel A., et al. Detailed modeling of skin penetration - an overview. Adv Drug Deliv Rev, 65:191-207, 2013.
- Yamaguchi K., et al. Analysis of in vitro skin permeation of 22-oxacalcitriol having a complicated metabolic pathway. Pharm Res, 23:680-8, 2006
- Yamaguchi K., et al. Analysis of in vitro skin permeation of 22-oxacalcitriol from ointments based on a two- or three-layer diffusion model considering diffusivity in a vehicle. Int J Pharm, 336:310-8, 2007.
- Yamaguchi K., et al. Skin permeation and metabolism of a new antipsoriatic vitamin D3 analogue of structure 16-en-22-oxa-24-carboalkoxide with low calcemic effect. Int J Pharm, 336:310-8, 2007.
- LeVeque, R. Finite Difference Methods for Ordinary and Partial Differential Equations, SIAM, 2007.
- LeVeque, R. Finite Volume Methods for Hyperbolic Problems. Cambridge University Press. ISBN 0-521-00924-3, 2002.

References

- Al-Qallaf, B., et al, Transdermal drug delivery by microneedles: does skin metabolism matter? International Journal of Chemical Reactor Engineering, 7, Article A69 (1-23), 2009.
- Koike Y., et al. Pharmacokinetics of Verapamil in Man. Research Communications in Chemical Pathology and Pharmacology, 37-47, 1979.
- Anderson P., et al. Clinical Pharmacokinetics of Verapamil in Patients with a Trial Fibrillation. European Journal of Clinical Pharmacology, 49-57, 1982.
- Eichelbaum M., et al. Simultaneous Determination of the Intravenous and Oral Pharmacokinetic Parameters of D, L-Verapamil Using Stable Isotope-labelled Verapamil. European Journal of Clinical Pharmacology, 133-137, 1981.
- Reits, E., et al. Peptide diffusion, protection, and degradation in nuclear and cytoplasmic compartments before antigen presentation by MHC class I. Immunity, 18(1):97-108, 2003.

Questions